

Research Paper

Modal frequency analysis for *Camellia oleifera* with sympodial branching growth mode using allometric scaling lawLewei Tang ^{a,b,*} Huiyu Zhang ^a, Shiyi Zhang ^a, Rui Pan ^a, Mingliang Wu ^{a,b}^a College of Mechanical and Electrical Engineering, Hunan Agricultural University, Changsha, 410128, China^b Specialty Oil Crop (*Camellia Oleifera*) Full Mechanization Research Centre, Changsha, 410128, China

ARTICLE INFO

Keywords:
 Modal frequency analysis
 Sympodial branching
 Allometric scaling law
 Tree model

ABSTRACT

In this paper, the branching growth mode of *Camellia oleifera* is considered to be a sympodial branching pattern. A simplified fractal model of *Camellia oleifera* is established with several similar basic units. The morphological parameters of the basic bifurcated units in the tree model are correlated according to the biological allometric scaling law. For the basic bifurcated unit, a cantilever trunk modelled as the Euler-Bernoulli beam with two lateral branches is obtained regardless of the mass of foliage. The modal frequency of the basic bifurcated unit is calculated using Hamilton's principle. Finite element simulation using ANSYS software is performed to obtain the simulation modal frequencies in comparison with the theoretical frequencies. An empirical formula relating to the modal frequencies is derived from the perspective of energy transfer. The effect of branch angle on the modal frequency is further investigated. Besides, the empirical formula is extended for the calculation of the modal frequency of three basic bifurcated units. The modal frequency in branch mode is also obtained and compared with the simulation results. In the field measurement, two coefficients involving the lateral branching ratio and the slenderness coefficient were identified from the morphological measurements. The modal frequency for the basic bifurcated unit and the tree were measured using the dynamic signal analyser. The relative errors of the modal frequency from the empirical formulas and the field experiments are less than 6 %, which demonstrates the feasibility of the modal frequency analysis of *Camellia oleifera* using the proposed empirical formulas.

Nomenclature

(continued)

a_1	$= 1.633 + 0.0426 \frac{l_1 \cos \varphi^b}{l_2}$
a_2	$= 1.633 + 0.0426 \frac{l_1 \cos \varphi^b}{l_3} + 0.1704 \frac{l_2}{l_3}$
A_2	Cross-section area of the main branch (m^2)
A_3	Cross-section area of the secondary branch (m^2)
β	Slenderness coefficient
d_k	Diameter of the k th branch (m)
dl	Infinitesimal length for the lateral branches (m)
ΔF	Variation of the external loading (N)
Δv	Variation of the maximum deflection (m)
E	Elastic modulus of the sample (Pa)
EI	Bending stiffness of the trunk ($\text{N}\cdot\text{m}^2$)
EI_2	Bending stiffness of the main branch ($\text{N}\cdot\text{m}^2$)
f_{br}	Modal frequency of the main branch in branch mode (Hz)
f_t	Modal frequency of the trunk in trunk mode (Hz)
k	Torsional elastic coefficient of the trunk ($\text{N}\cdot\text{m}\cdot\text{rad}^{-1}$)

(continued on next column)

l_1	Length of the trunk (m)
l_2	Length of the lateral branches (m)
l_k	Length of the k th branch (m)
λ	Area reduction coefficient
m	Mass of the trunk (kg)
m_2	Mass of one main branch (kg)
M	Mass of the tip (kg)
ω	Circular modal frequency ($\text{rad}\cdot\text{s}^{-1}$)
R	Rotational matrix from the global coordinate system to the relative coordinate system
$\mathbf{r}_{dl-\text{right/left}}$	Displacement vector of an infinitesimal length dl for the right/left lateral branch (m)
$\dot{\mathbf{r}}_{dl-\text{right/left}}$	Velocity of an infinitesimal length dl for the right/left lateral branch ($\text{m}\cdot\text{s}^{-1}$)
\mathbf{r}_P	Displacement vector at node P' in the global coordinate system (m)
$\theta_O(l_1, t)$	Angle between the trunk axis and the line $O P'$ (rad)
$\theta_O'(l_1, t)/\theta_O$	Inclination angle of the trunk axis at node P' to the Y-axis (rad)
$\dot{\theta}_O$	First derivative of angle θ_O with respect to time t ($\text{rad}\cdot\text{s}^{-1}$)

(continued on next page)

* Corresponding author. College of Mechanical and Electrical Engineering, Hunan Agricultural University, Changsha, 410128, China.

E-mail addresses: tanglw@hunau.edu.cn (L. Tang), mlwu@hunau.edu.cn (M. Wu).

(continued)

$\ddot{\theta}_o$	Second derivative of the angle θ_o with respect to time t ($\text{rad}\cdot\text{s}^{-2}$)
τ	$= \frac{\omega^2 \rho_1}{EI}$
T_{br}	Kinetic energy of two lateral branches in the trunk mode (J)
T_{l2}	Kinetic energy of two lateral branches (J)
T_{l3}	Kinetic energy of four secondary lateral branches (J)
T_{trunk}	Kinetic energy of the trunk (J)
ϕ^b	Angle of a lateral branch to the trunk axis ($^\circ$)
ρ	Density of <i>Camellia oleifera</i> ($\text{kg}\cdot\text{m}^{-3}$)
ρ_1	Mass per unit length of the trunk ($\text{kg}\cdot\text{m}^{-1}$)
ρ_2	Mass per unit length of the lateral branches ($\text{kg}\cdot\text{m}^{-1}$)
V	Elastic potential energy of the trunk (J)
$v(l_1, t)$	Instantaneous deflection from node P to node P' (m)
v'	Derivative of instantaneous deflection v with respect to length l
\dot{v}	Instantaneous velocity at node P' ($\text{m}\cdot\text{s}^{-1}$)
\ddot{v}	Derivative of instantaneous velocity with respect to length l (s^{-1})
\ddot{v}	Instantaneous acceleration at node P' ($\text{m}\cdot\text{s}^{-2}$)
\ddot{v}	Derivative of instantaneous acceleration with respect to length l (s^{-2})
v_{dl}	Linear velocity for the infinitesimal mass dl ($\text{m}\cdot\text{s}^{-1}$)
$v_{dl_{2-rr/l/r/l/r}}$	Linear velocity for the left/right secondary branch of the left/right main branch respectively ($\text{m}\cdot\text{s}^{-1}$)
v_{dl}^r	Relative velocity from the angular velocity at node P' ($\text{m}\cdot\text{s}^{-1}$)
v_P	Linear velocity at node P' ($\text{m}\cdot\text{s}^{-1}$)
$\Psi(l)$	Expression only related to the location of the curvilinear points l

1. Introduction

Camellia oleifera (hereafter *C. oleifera*) originates from southern China and has been cultivated as an economic oil crop for more than 2300 years (Luan et al., 2020; Quan et al., 2022). *C. oleifera* (*oleifera* oil) together with *E. guineensis* (palm oil), *O. europaea* (olive oil) and *C. nucifera* (coconut oil) are widely recognised as four major sources for edible woody oil all over the world (Zhang et al., 2019). Oleifera oil extracted from *C. oleifera* seeds contains abundant bioactive substances and unsaturated fatty acids, which are comparable to olive oil and beneficial to human health (Gao et al., 2024). *C. oleifera* is a subtropical evergreen tree and mostly distributed in the south of China. The total *C. oleifera* planting area in China was 4.7 million hm^2 in 2022 and the recent plan is to increase it to 6 million hm^2 in 2025 (Zhang et al., 2022). Thus, the full mechanization development of *C. oleifera* production becomes a significant solution to ensure a sustainable supply of high-quality edible oil in China.

C. oleifera fruit ripens seasonally from September to November and the fruit ripening period coincides with the flowering period ranging from October to February (Gao et al., 2015). The commonly used harvest method for *C. oleifera* fruit still largely relies on manual hand-picking labour. The labour-intensive harvesting has some critical disadvantages such as low harvest efficiency (Du et al., 2021). In the recent literature (Castro-Garcia et al., 2012; Hoshyanmanesh et al., 2017; Jiao et al., 2024; Li et al., 2018; Zheng et al., 2023), the vibratory harvesting technology has been attempted in tree fruit harvest. Castro-Garcia et al. (2012) studied the effects of both excitation frequency and vibrating duration on the harvest efficiency of pine nuts. It confirms the potential relationship between the harvest efficiency and the dynamic characteristics of pines. Hoshyanmanesh et al. (2017) investigated the optimised shaking frequency of 20 Hz to acquire the maximum harvest rate of olive trees. A vibration model of fruit tree branches as well as natural frequencies are proposed (Jiao et al., 2024). A hybrid shaking-fixed combo picker was invented for litchi harvest with the vibration frequency of 20 Hz (Li et al., 2018). The shaking position of an existing catch-and-shake harvester for jujube fruit was determined in a deep learning framework (Zheng et al., 2023). Zhou et al. (2022) used a finite element model to trigger sub-harmonic resonance of the ginkgo seed-stem system. These works have demonstrated that the vibratory harvesting is a suitable approach for tree fruits. However, the determination of the vibration frequency highly depends on in-situ experiments and finite element models without a valid theoretical frequency deduction. More importantly, the vibration harvesting has been proved

to be feasible for *C. oleifera* fruit with high efficiency (Du, Ning, et al., 2022; Du, Shen, et al., 2022; Wu et al., 2022; Yan et al., 2023). Modal analysis of the *C. oleifera* trees with three types of canopy shapes was implemented in ANSYS software and the fundamental modal frequency ranged between 1 Hz and 2 Hz (Du, Shen, et al., 2022). The optimal vibration frequency for harvesting *C. oleifera* fruits was obtained as 7.18 Hz based on energy transfer characteristics (Wu et al., 2022). The crawler-type high clearance vibratory harvester for *C. oleifera* adopted the excitation frequency of 6 Hz in the field experiments (Du, Chen, et al., 2022). Similar to Li et al. (2018), a hand-held impacting comb-type harvester was used with the vibration frequency of 6.8 Hz to achieve the best device performance (Yan et al., 2023). The robotic harvesting system with vision recognition algorithm may be considered as a supplement for *C. oleifera* fruit harvest (Chen et al., 2023; Droukas et al., 2023; Zheng et al., 2020). To summarise, the aforementioned references have validated that the vibratory harvesting for *C. oleifera* works well in the existing prototypes. But the theoretical determination of the excitation frequency for *C. oleifera* fruits still needs to be further solved, which will benefit for the control system design of the vibratory harvesting equipment.

To ease of detaching the tree fruits, the *C. oleifera* branches are expected to resonate near the excitation frequency. It means the excitation frequency needs to be close to the modal frequencies of *C. oleifera* trees. The commonly used modal frequency analysis of trees includes dynamic modelling (James et al., 2006; Lang, 2008; Lang & Csorba, 2015; Murphy & Rudnicki, 2012) and simulation together with in-situ experiment testing (Du, Chen, et al., 2022; Du, Shen, et al., 2022; Hoshyanmanesh et al., 2017; Li et al., 2018; Wu et al., 2022; Yan et al., 2023). The optimum excitation frequency for *C. oleifera* trees is in the range of 6–7 Hz (Du, Chen, et al., 2022; Du, Shen, et al., 2022; Wu et al., 2022; Yan et al., 2023), while the vibration frequency for litchi/olive trees is around 20 Hz (Hoshyanmanesh et al., 2017; Li et al., 2018). The difference in frequency may be explained from the corresponding tree models of various tree species. Generally, the branching growth modes directly affect the branch distribution of the tree architecture. The modes of branching for several tree species are classified into monopodial mode and sympodial mode (Lopez et al., 2011; Rodriguez et al., 2008). Referring to Wu et al. (2022), the branches of *C. oleifera* trees grow in sympodial mode, which is described that a trunk of *C. oleifera* is always separated into two lateral branches. A basic bifurcated unit (a Y-shaped branched unit) composed of a trunk and two lateral branches was analysed using a mass-spring model (Theckes et al., 2011). Two typical modes used in the vibration analysis of Y-shaped branched trees are the “trunk mode” and the “damped branch mode”. In the trunk mode, it is assumed that only the trunk bends, while the branches remain still with respect to the trunk (Fig. 5b). In branch mode, the trunk is assumed to stay fixed, while the branches oscillate and bend (Fig. 5c). Wu et al. (2022) proposed a mass-spring-damper model with five degrees of freedom for *C. oleifera* involving a trunk, two primary lateral branches and two secondary lateral branches. The deduction process is difficult to be applied to the entire *C. oleifera* tree architecture formed by multiple Y-shaped branched units. Weng and Xu (2013) established a Y-trellis tree model by simplifying a wedge-shaped tree into a cylinder tree with a mass loading fixed at the tip. Ma et al. (2022) presented a mathematical modelling of vibration transfer in Pistachio trees with accelerometers. A three-dimensional model of an olive tree considering branches was established for determination of the optimal vibration parameters in Niu et al. (2022). In our previous work (Tang, Gouttefarde, Doria, et al., 2022; Tang, Gouttefarde, Sun, et al., 2021), the modal frequencies of a flexible single-link with two cables were obtained using a cantilever beam model with a tip mass. Bejan et al. (2008) showed the basis features of tree architecture with the hierarchical distribution of canopy size and conical branches can be expressed in a unifying basis. In theory, the tree with sympodial branches can be modelled as an infinite iterated fractal tree. Loong and Dimitrakopoulos (2023, 2024) proposed an analytical approach to examine the modal frequencies of the fractal

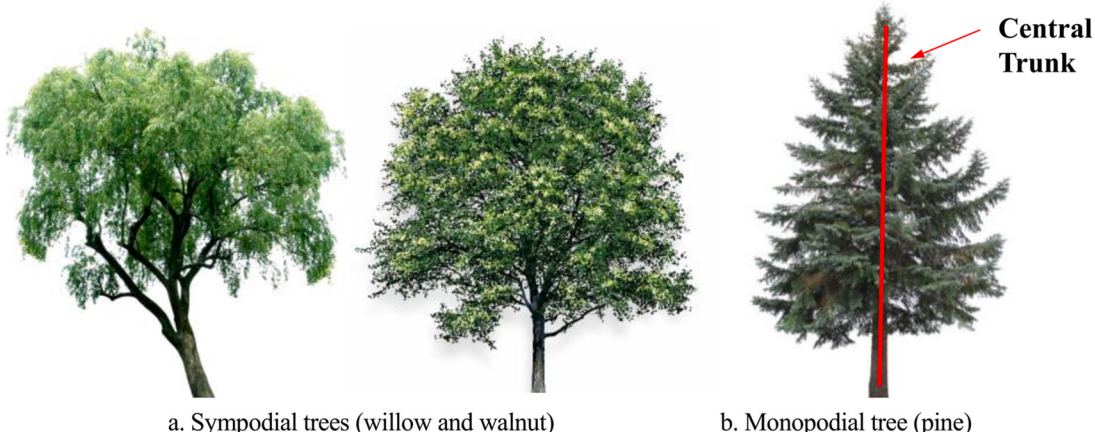


Fig. 1. Typical trees in two branching growth patterns.



Fig. 2. *C. oleifera* tree.

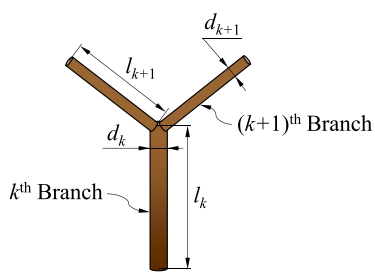


Fig. 3. Morphological parameters of two branches in k^{th} and $(k+1)^{\text{th}}$ order.

sympodial trees. The numerical simulation was provided but no in-situ experiments were implemented. Recently, dynamic response and modal frequency identification of *C. oleifera* had been investigated with high-speed photography and back propagation neural network in Wang et al. (2024) & Du et al. (2024). In this paper, the modal frequency analysis of *C. oleifera* is performed based on energy transfer mechanism. Hamilton's principle is employed to derive the governing differential equations of motion for the basic bifurcated unit. More importantly, an

empirical formula is proposed to calculate the modal frequencies of the fractal sympodial tree in hierarchical order.

The main contribution of this paper includes: (1) the derivation of a simplified fractal sympodial tree model for *C. oleifera* with in-situ experiments; (2) the theoretical deduction of the modal frequencies in the trunk mode for the basic bifurcated unit; (3) the proposed empirical formula of the model frequencies for the proposed *C. oleifera* tree in hierarchical order. In comparison with the abovementioned relevant research works, this paper provides the mathematical tree model of *C. oleifera*, which can highly avoid the time-consuming approach using the finite element model. Based on this fractal sympodial tree model, the model frequencies both in trunk mode and branch mode can be calculated with feasible accuracy. The results of this paper will be used to determine the optimum excitation frequency for the design of *C. oleifera* fruit harvester.

2. Materials and methods

2.1. Simplified fractal tree model using allometric scaling law

Branches of different tree species usually grow in their own patterns. A typical tree architecture consists of a trunk, lateral main branches, sub-branches, small twigs and leaves. Two distinct types of tree architectures are referred to be sympodial and monopodial. In general, a sympodial tree such as a willow or walnut has no central trunk in Fig. 1a, while a monopodial tree has an axial central trunk such as a pine shown in Fig. 1b.

The morphological observation of *C. oleifera* trees in Fig. 2 shows that the branches of *C. oleifera* trees grow in a sympodial pattern. Each branch segment of *C. oleifera* is usually separated into two lateral secondary branches at a branch tip. Thus, the simplified fractal tree model of *C. oleifera* can be described by branches in hierarchical order, where the cross-section and the length of each branch satisfy certain biological growth laws. It can be noted that the branches with foliage have a significant influence on dynamic response under forced vibration (Sola-Guirado et al., 2022). Furthermore, the dynamic vibration characteristics of centuries-old olive trees are primarily affected by the foliage due to the remarkable aerodynamic damping (Camposeo et al., 2023). However, the damping resulting from the aerodynamic drag on the foliage exerts a negligible effect on the modal frequencies of trees. Therefore, the architecture of trees without leaves is investigated in this paper, which follows the same assumption in Du et al. (2024) & Lopez et al. (2011).

Biological structures of living things usually fulfil a certain allometric scaling law (West et al., 1997, 1999). More specifically, the diameters of the main branch and two lateral branches conform with Leonardo's rule (Eloy, 2011) involving two critical coefficients. One is the area reduction

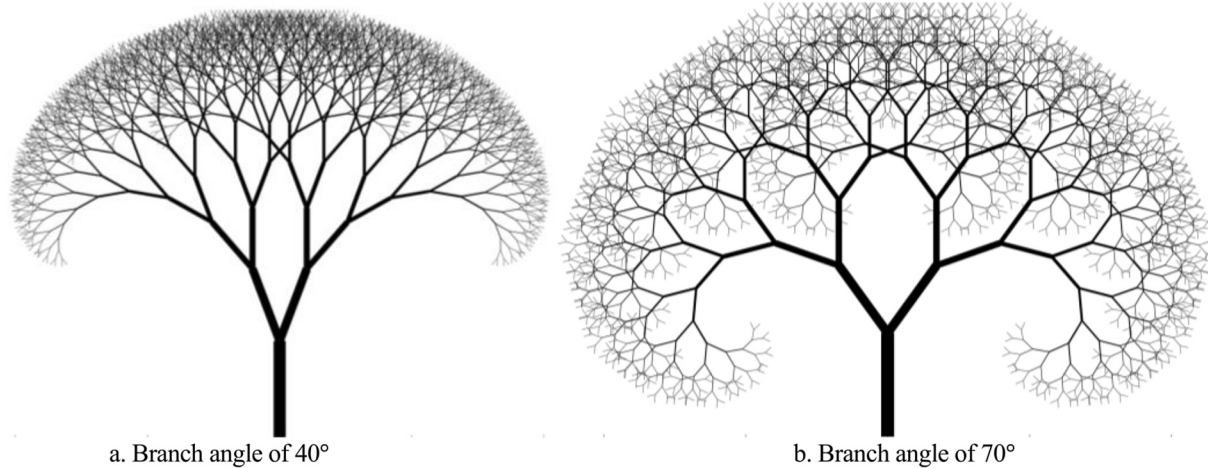


Fig. 4. Simplified fractal tree architectures with $\lambda = 0.5$, $\beta = 1.5$ and branch angles {40 °, 70 °}.

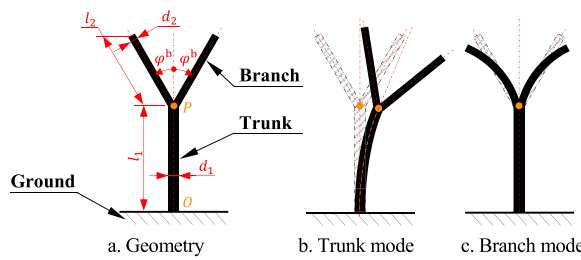


Fig. 5. Geometrical description of a basic bifurcated unit and its bending modes.

coefficient λ , which denotes the reduction of the lateral branch diameters compared to the main branch diameter. The other is the slenderness coefficient β describing the relationship of the lengths and the diameters of two branches in a hierarchical order. As depicted in Fig. 3, a basic bifurcated unit of a sympodial tree is composed of a k th main branch and two $(k+1)^{\text{th}}$ lateral branches. The three branches are assumed to be in the same plane and the shape of each branch is simplified as a cylinder. Moreover, two lateral branches at the same branching node are assumed to grow symmetrically to the axis of the main branch. The branch angle is defined as the angle of two lateral branches. The branch sizes of the fractal tree model are expressed in terms of the branch diameter and the branch length. The relationship between the branch diameters and the branch lengths is represented as follows.

$$\lambda = \left(\frac{d_{k+1}}{d_k} \right)^2, \quad (1)$$

$$\frac{d_{k+1}}{d_k} = \left(\frac{l_{k+1}}{l_k} \right)^\beta, \quad (2)$$

where $\{d_k, d_{k+1}\}$ and $\{l_k, l_{k+1}\}$ denote the diameters and the lengths of the k th branch and the $(k+1)^{\text{th}}$ branch respectively. Referring to Rodriguez et al. (2008), the parameter ranges in the allometric scaling law for sympodial trees is constrained as $\lambda < 1$ and $1 < \beta < 2$. For example, two fractal tree architectures following the allometric scaling law with $\lambda = 0.5$ and $\beta = 1.5$ as well as two different branch angles {40 °, 70 °} are depicted in Fig. 4.

2.2. Dynamic model of a basic bifurcated unit

As illustrated in Fig. 5, a basic bifurcated unit is formed by a trunk

and two lateral branches connected at node P . The trunk is fixed to the ground at node O . Two lateral branches are symmetrically distributed and each branch is at an angle ϕ^b to the trunk axis as shown in Fig. 5a. The material of both the trunk and branches is assumed to be linearly elastic and homogeneous. Following the references (Rodriguez et al., 2008; Theckes et al., 2011), only the trunk mode (Fig. 5b) and the branch mode (Fig. 5c) are studied in this paper. Two modes of the basic bifurcated unit reflect bending deformation of the trunk and the lateral branches respectively. In trunk mode, the trunk bends and then takes two lateral branches to move together as a rigid body. It means that in trunk mode the elastic potential energy of the trunk and the kinetic energy of both the trunk and two lateral branches are transferred between each other. In branch mode, only two lateral branches bend and the trunk always remain still. In other words, two lateral branches are considered to be steadily fixed at node P in the branch mode.

From the field observation, the trunk and branches of *C. oleifera* trees are represented as slender Euler-Bernoulli beams. Considering the ground constraint, a basic bifurcated unit is further described as a cantilever beam with two lateral rigid branches in trunk mode. Similarly, a lateral branch of the basic bifurcated unit in branch mode is considered as a cantilever beam without tip mass.

Spatz et al. (2007) presented the fourth-order differential equation for the bending oscillation of a slender beam without tip mass. In our previous work (Tang, Gouttefarde, Doria, et al., 2022; Tang, Gouttefarde, Sun, et al., 2021), the modal analysis of a flexible single-link with two cables is performed using Hamilton's principle. However, the results of these works cannot be directly applied to the modal analysis of the present basic bifurcated unit. A related work concerning the dynamic modelling of a slender beam with non-tip mass was presented and validated numerically (Oguamanam, 2003). In this work, a detailed deduction of the boundary constraints at node P is provided by finding the expression of the kinetic energy for two lateral branches in the trunk mode.

As illustrated in Fig. 6, the global Cartesian coordinate system is defined with the origin at node O . The direction of the Y -axis is set along the axis of the trunk upwards, and the direction of the X -axis is perpendicular to that of the Y -axis. Let $v(l_1, t)$ denote an instantaneous deflection at node P in the trunk mode as a function of time t and the trunk length l_1 . Based on the small oscillation assumption in free vibration, the position of node P in the global coordinate system at a given instant of time t is represented as $\mathbf{r}_P = [v(l_1, t), l_1]^T$. The angle $\theta_O(l_1, t)$ is used to indicate the angle of inclination of the trunk axis at the node P to the Y -axis during vibration.

The positions of an infinitesimal length dl for the left and right lateral branches are presented in the global coordinate system as

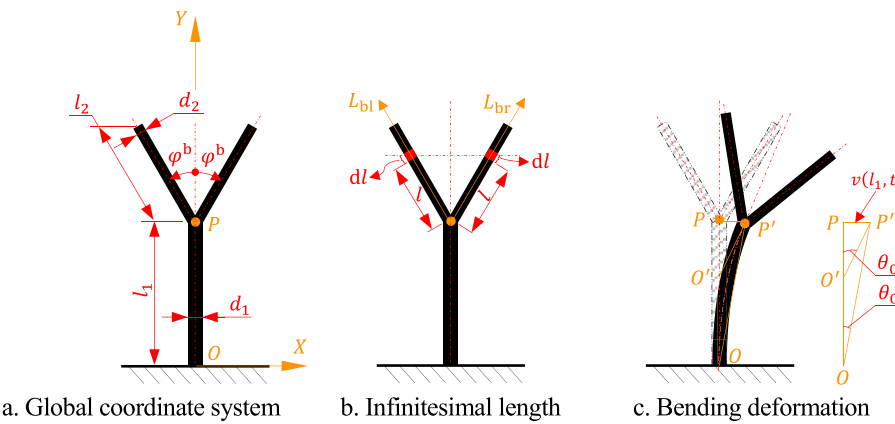


Fig. 6. Bending deformation of two lateral branches in global coordinate system.

$$\begin{cases} \mathbf{r}_{dl-right} = \mathbf{r}_P + \mathbf{R}[l \sin \varphi^b, l \cos \varphi^b]^T, \\ \mathbf{r}_{dl-left} = \mathbf{r}_P + \mathbf{R}[-l \sin \varphi^b, l \cos \varphi^b]^T, \end{cases} \quad (3)$$

where the rotational matrix $\mathbf{R} = \begin{bmatrix} \cos(\theta_O(l_1, t)) & \sin(\theta_O(l_1, t)) \\ -\sin(\theta_O(l_1, t)) & \cos(\theta_O(l_1, t)) \end{bmatrix}$. Furthermore, the expression of positions in Eq. (3) are simplified using trigonometric functions as

$$\begin{cases} \mathbf{r}_{dl-right} = [v(l_1, t) + l \sin(\theta_O(l_1, t) + \varphi^b), l_1 + l \cos(\theta_O(l_1, t) + \varphi^b)]^T, \\ \mathbf{r}_{dl-left} = [v(l_1, t) + l \sin(\theta_O(l_1, t) - \varphi^b), l_1 + l \cos(\theta_O(l_1, t) - \varphi^b)]^T. \end{cases} \quad (4)$$

By taking the time derivation of both sides of Eq. (4), the velocity of the infinitesimal length dl is obtained as

$$\begin{cases} \dot{\mathbf{r}}_{dl-right} = [\dot{v} + \dot{\theta}_O l \cos(\theta_O + \varphi^b), -\dot{\theta}_O l \sin(\theta_O + \varphi^b)]^T, \\ \dot{\mathbf{r}}_{dl-left} = [\dot{v} + \dot{\theta}_O l \cos(\theta_O - \varphi^b), -\dot{\theta}_O l \sin(\theta_O - \varphi^b)]^T, \end{cases} \quad (5)$$

where the trunk length l_1 and time t of both v and θ_O are omitted for simplicity unless explicitly stated otherwise. The kinetic energy of two lateral branches in the trunk mode are derived as

$$T_{br} = \frac{1}{2}\rho_2 \int_0^{l_2} \dot{\mathbf{r}}_{dl-right}^T \dot{\mathbf{r}}_{dl-right} dl + \frac{1}{2}\rho_2 \int_0^{l_2} \dot{\mathbf{r}}_{dl-left}^T \dot{\mathbf{r}}_{dl-left} dl. \quad (6)$$

where ρ_2 is the mass per unit length of the lateral branch and l_2 is the lateral branch length. After several mathematical manipulations, the expression of the kinetic energy for two lateral branches is obtained as

$$T_{br} = \rho_2 l_2 \dot{v}^2 + \frac{l_2^3}{3} \rho_2 \dot{\theta}_O^2 + \rho_2 l_2^2 \cos \varphi^b \dot{v} \dot{\theta}_O \cos \theta_O. \quad (7)$$

As a result, the variation of the kinetic energy in Eq. (7) is given as follows

$$\delta T_{br} = \rho_2 l_2 \left[2\dot{v} \delta \dot{v} + \frac{2l_2^2}{3} \dot{\theta}_O \delta \dot{\theta}_O + l_2 \cos \varphi^b (-\dot{v} \dot{\theta}_O \sin \theta_O \delta \theta_O + \dot{v} \cos \theta_O \delta \dot{\theta}_O + \dot{\theta}_O \cos \theta_O \delta \dot{v}) \right]. \quad (8)$$

Because the bending deformation of the trunk in the trunk mode along the trunk length is continuously differentiable, the relationship between θ_O and v is expressed as $\tan \theta_O = v'$. Hereafter, the prime ($'$) means the derivative with respect to the length l . When the angle θ_O is assumed as a minute quantity, the equation $\tan \theta_O \approx \theta_O = v'$ holds and then $\cos \theta_O \approx 1$. As a result, the boundary constraint equations of force and moment equilibrium at node P' are in accord with the results in Ogumananam (2003).

Owing to the effect of the lateral branches, the angle θ_O is kept as a

quantity with moderate value rather than a truly minute quantity. Thus, two following equations associated with the angle θ_O are obtained.

$$\begin{cases} \sin \theta_O = \frac{v'}{\sqrt{1 + (v')^2}}, \\ \cos \theta_O = \frac{1}{\sqrt{1 + (v')^2}}. \end{cases} \quad (9)$$

Using the time derivative of both sides of $\tan \theta_O = v'$, the first derivative and the second derivative of the angle θ_O with respect to time are generated as

$$\begin{cases} \dot{\theta}_O = \frac{\dot{v}'}{1 + v'^2}, \\ \ddot{\theta}_O = \frac{\ddot{v}'(1 + v'^2) - 2\dot{v}'^2 v'}{(1 + v'^2)^2}. \end{cases} \quad (10)$$

By substituting Eq. (9) and Eq. (10) into Eq. (8), the variation of the kinetic energy is rewritten as

$$\delta T_{br} = \rho_2 l_2 \left[2\ddot{v} \delta v + \frac{2l_2^2}{3} (\ddot{v}' + \dot{v}' v'^2 - 2\dot{v}'^2 v') \delta \theta_O + l_2 \cos \varphi^b (-\dot{v} \dot{v}' \delta \theta_O + \dot{v}') \right]. \quad (11)$$

Referring to (Tang, Gouttefarde, Doria, et al., 2022; Tang, Gouttefarde, Sun, et al., 2021), the bending deflection $v(l, t)$ along the length of the trunk is assumed to be separable in space and time, which is expressed as $v(l, t) = \Psi(l) \sin(\omega t)$ and ω denotes the circular modal frequency. The general solution of $\Psi(l)$ is given as

$$\Psi(l) = A \sin(\tau l) + B \cos(\tau l) + C \sinh(\tau l) + D \cosh(\tau l), \quad (12)$$

where $\tau^4 = \frac{\omega^2 \rho_1}{EI}$, ρ_1 is the mass per unit length of the trunk, EI denotes the bending stiffness of the trunk and $\{A, B, C, D\}$ are four unknown coefficients related to $\Psi(l)$. Based on Eq. (11), the boundary constraint equations of force and moment equilibrium at node P' are obtained as below,

$$-EIv''' + 2\rho_2 l_2 \ddot{v} + \rho_2 l_2^2 \cos \varphi^b \ddot{v}' = 0, \quad (13)$$

$$EIv'' + \frac{2l_2^3}{3} \rho_2 (\ddot{v}' + \dot{v}' v'^2 - 2\dot{v}'^2 v') + \rho_2 l_2^2 \cos \varphi^b (-\dot{v} \dot{v}' \delta \theta_O + \dot{v}') = 0. \quad (14)$$

After substituting Eq. (12) into Eq. (14), Eq. (14) is simplified as

$$EIv'' + \frac{2l_2^3}{3} \rho_2 \left(1 + \frac{1}{6} + \frac{l_1}{8l_2} \cos \varphi^b \right) \ddot{v}' + \rho_2 l_2^2 \cos \varphi^b \ddot{v} = 0. \quad (15)$$

Together with another two boundary conditions at node O , four boundary constraints of the trunk for the basic bifurcated unit are assembled as

$$\underbrace{\begin{bmatrix} 0 & 1 & 0 & 1 \\ 1 & 0 & 1 & 0 \\ H_{11} & H_{12} & H_{13} & H_{14} \\ H_{21} & H_{22} & H_{23} & H_{24} \end{bmatrix}}_{\boldsymbol{\Pi}} \begin{bmatrix} A \\ B \\ C \\ D \end{bmatrix} = \begin{bmatrix} 0 \\ 0 \\ 0 \\ 0 \end{bmatrix}, \quad (16)$$

where

$$H_{11} = -k \sin(\tau l_1) - \frac{2l_2^3}{3} \left(1 + \frac{1}{6} + \frac{l_1}{8l_2} \cos \varphi^b \right) \tau^3 \cos(\tau l_1) - l_2^2 \cos \varphi^b \tau^2 \sin(\tau l_1),$$

$$H_{12} = -k \cos(\tau l_1) + \frac{2l_2^3}{3} \left(1 + \frac{1}{6} + \frac{l_1}{8l_2} \cos \varphi^b \right) \tau^3 \sin(\tau l_1) - l_2^2 \cos \varphi^b \tau^2 \cos(\tau l_1),$$

$$H_{13} = k \sinh(\tau l_1) - \frac{2l_2^3}{3} \left(1 + \frac{1}{6} + \frac{l_1}{8l_2} \cos \varphi^b \right) \tau^3 \cosh(\tau l_1) - l_2^2 \cos \varphi^b \tau^2 \sinh(\tau l_1),$$

$$H_{14} = k \cosh(\tau l_1) - \frac{2l_2^3}{3} \left(1 + \frac{1}{6} + \frac{l_1}{8l_2} \cos \varphi^b \right) \tau^3 \sinh(\tau l_1) - l_2^2 \cos \varphi^b \tau^2 \cosh(\tau l_1),$$

$$H_{21} = 2\tau l_2 \sin(\tau l_1) - k \cos(\tau l_1) + l_2^2 \cos \varphi^b \tau^2 \cos(\tau l_1),$$

$$H_{22} = 2\tau l_2 \cos(\tau l_1) + k \sin(\tau l_1) - l_2^2 \cos \varphi^b \tau^2 \sin(\tau l_1),$$

$$H_{23} = 2\tau l_2 \sinh(\tau l_1) + k \cosh(\tau l_1) + l_2^2 \cos \varphi^b \tau^2 \cosh(\tau l_1),$$

$$H_{24} = 2\tau l_2 \cosh(\tau l_1) + k \sinh(\tau l_1) + l_2^2 \cos \varphi^b \tau^2 \sinh(\tau l_1) \text{ and } k = \frac{d_1^2}{d_2^2}.$$

To obtain a non-trivial solution of the unknown coefficient vector $[A, B, C, D]^T$ in Eq. (16), the determinant of the matrix $\boldsymbol{\Pi}$ needs to be zero. Thus, a nonlinear transcendental equation involving variable τ is derived from the condition that the determinant of matrix $\boldsymbol{\Pi}$ is equal to zero. After finding the value of variable β , the circular modal frequency of the basic bifurcated unit in the trunk mode is calculated by $\omega = \tau^2 \sqrt{\frac{EI}{\rho_1}}$.

2.3. Empirical formula of modal frequency

In the proposed theoretical method, a transcendent equation involving the modal frequencies is solved by the fzero function in MATLAB software. For ease of calculation, an empirical formula is presented for determining the modal frequency in the trunk mode for the basic bifurcated unit. If a cantilever beam with its mass of m and a tip mass of M is considered, then the modal frequency in the trunk mode for the cantilever beam is obtained using the following formula (Tang, Gouttefarde, Sun, et al., 2021).

$$f_t = \frac{1}{2\pi} \sqrt{\frac{3EI}{\left(M + \frac{33}{140}m \right) l^3}} \quad (17)$$

Since two lateral branches are not able to be assumed as a tip mass for a basic bifurcated unit, the kinetic energy of two lateral branches is expressed using integral along the lateral branch length. Referring to Wang (1965), the torsional elastic coefficient of the trunk with the length of l_1 and the bending stiffness of EI is represented as

$$k = \frac{3EI}{l_1}. \quad (18)$$

Therefore, the elastic potential energy of the trunk in the trunk mode is obtained as $V = \frac{1}{2}k\theta_0^2$, where θ_0 denotes the instantaneous inclination angle of the line OP' with respect to the Y -axis in the global coordinate system. Based on the empirical formula in Eq. (17), the kinetic energy of the trunk with the instantaneous bending deformation is assumed as

$$T_{\text{trunk}} = \frac{1}{2} \left(\frac{33}{140}m \right) \dot{\theta}_0^2 l_1^2. \quad (19)$$

The value of the linear velocity at node P' is written as

$$\|\mathbf{v}_P\| = \dot{\theta}_0 l_1. \quad (20)$$

The kinetic energy T_{l2} of two lateral branches is generated as

$$T_{l2} = A_2 \rho \int_0^{l_2} \|\mathbf{v}_{dl}\|^2 dl, \quad (21)$$

where A_2 is the cross-section area of the lateral branch and ρ is the density of *C. oleifera*. As shown in Fig. 7, the notation $\|\mathbf{v}_{dl}\|$ denotes the norm of the linear velocity for the infinitesimal mass dl along the lateral branch and is expressed as

$$\|\mathbf{v}_{dl}\| = \sqrt{\|\mathbf{v}_P\|^2 + \|\mathbf{v}_{dl}^r\|^2 + 2\|\mathbf{v}_P\|\|\mathbf{v}_{dl}^r\|\cos \varphi^b}, \quad (22)$$

where $\|\mathbf{v}_{dl}^r\| = a_1 \dot{\theta}_0 l$, the angular velocity at node P' is defined as $\dot{\theta}_0 = a_1 \dot{\theta}_0$ and a_1 is an unknown coefficient. Using Hamilton's principle, the modal frequency of the basic bifurcated unit in trunk mode is obtained as

$$f_t = \frac{1}{2\pi} \sqrt{\frac{3EI}{\frac{33}{140}ml_1^3 + 2A_2\rho \left(l_2 l_1^3 + \frac{1}{2}l_2^3 l_1 a_1^2 + a_1 l_1^2 l_2^2 \cos \varphi^b \right)}}. \quad (23)$$

The detailed derivation of Eq. (23) is added in the Appendix. It demonstrates that the circular modal frequency of the basic bifurcated unit in the trunk mode is related to the bending stiffness EI , the lengths and the diameters of both the trunk and the lateral branch as well as the branch angle φ^b . In this paper, it is assumed that the left and the right lateral branches are identical. In practice, the left and right branches are generally of different diameters and lengths. The proposed theoretical method remains valid using the kinetic energy of the two different branches.

Subsequently, the kinetic energy of all branches except for the trunk needs to be investigated further. Firstly, a simplified tree model with three basic bifurcated units is introduced and its corresponding morphological dimensions are illustrated in Fig. 8.

The value of the linear velocity for the infinitesimal mass dl along the main branch is the same as Eq. (22). Subsequently, the values of the linear velocity for the infinitesimal mass dl_2 for four secondary branches are obtained as

$$\begin{aligned} \|\mathbf{v}_{dl_2-l}\| &= \|\mathbf{v}_{dl_2-r}\| = \sqrt{\|\mathbf{v}_P\|^2 + \|\mathbf{v}_{dl_2}^r\|^2 + 2\|\mathbf{v}_P\|\|\mathbf{v}_{dl_2}^r\|\cos(2\varphi^b - \phi)}, \\ \|\mathbf{v}_{dl_2-l}\| &= \|\mathbf{v}_{dl_2-r}\| = \sqrt{\|\mathbf{v}_P\|^2 + \|\mathbf{v}_{dl_2}^r\|^2 + 2\|\mathbf{v}_P\|\|\mathbf{v}_{dl_2}^r\|\cos \phi}, \end{aligned} \quad (24)$$

where the notations $\{ll, lr, rl, rr\}$ denote the left/right secondary branch of the left/right main branch respectively, the relative linear velocity due to the angular velocity $\|\mathbf{v}_{dl_2}^r\| = a_2 \dot{\theta}_0 \sqrt{l_2^2 + l^2 + 2ll_2 \cos \varphi^b}$, $\cos \phi = \frac{l+l_2 \cos \varphi^b}{\sqrt{l_2^2 + l^2 + 2ll_2 \cos \varphi^b}}$, $\sin \phi = \frac{l_2 \sin \varphi^b}{\sqrt{l_2^2 + l^2 + 2ll_2 \cos \varphi^b}}$, $\cos(2\varphi^b - \phi) = \cos(2\varphi^b)\cos \phi + \sin(2\varphi^b)\sin \phi$ and a_2 is another unknown coefficient. The kinetic energy T_{l3} of four secondary lateral branches is yielded as

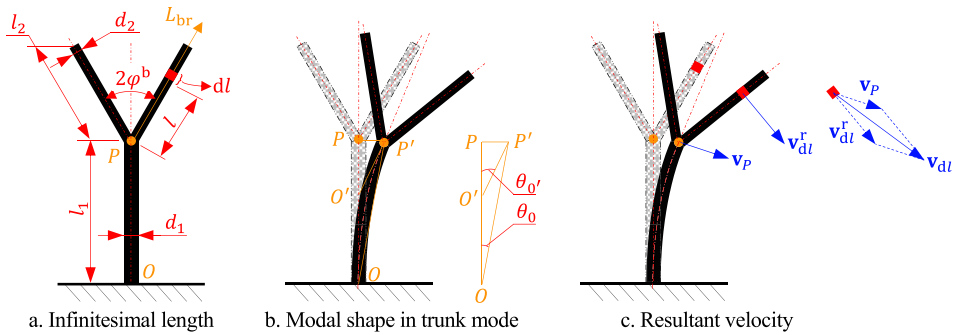


Fig. 7. Resultant velocity of the infinitesimal mass dl for the lateral branch.

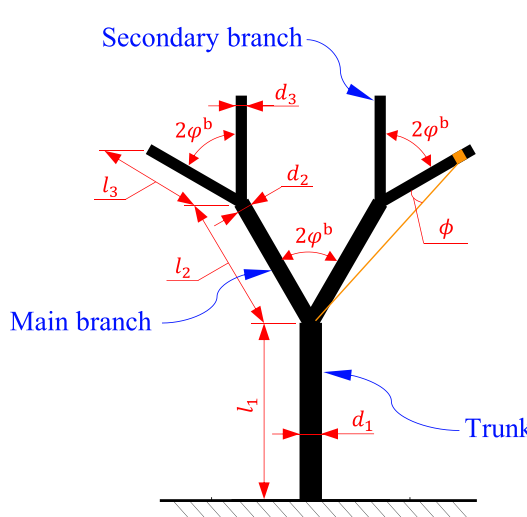


Fig. 8. Dimensions of a simplified tree model with three basic bifurcated units.

$$T_{13} = A_3 \rho \int_0^{l_3} (\|v_{dl_2-l}\|^2 + \|v_{dl_2-lr}\|^2) dl_2, \quad (25)$$

where A_3 is the cross-section area of four secondary lateral branches. Consequently, the modal frequency of three basic bifurcated units in the trunk mode is obtained as

$$f_t = \frac{1}{2\pi} \sqrt{\frac{3EI}{\frac{33}{140}m_2l_2^3 + 2A_2\rho(l_2l_1^3 + \frac{1}{3}l_2^3l_1a_2^2 + a_2l_1^2l_2^2 \cos \varphi^b) + J_{b2}l_2}}, \quad (26)$$

where $J_{b2} = A_3\rho [4l_3l_1^2 + \frac{4}{3}l_3^3a_2^2 + 4a_2^2l_3l_2^2 + 4a_2^2l_3^2l_2 \cos \varphi^b + 4a_2l_1\sqrt{l_2^2 + l_2^2 + 2ll_2 \cos \varphi^b} \cos \phi + 4a_2l_1\sqrt{l_2^2 + l_2^2 + 2ll_2 \cos \varphi^b} \cos(2\varphi^b - \phi)]$. After substituting the expression of $\sin\phi$ and $\cos\phi$, J_{b2} can be further derived as

$$J_{b2} = 4A_3\rho \left[l_3l_1^2 + \frac{1}{3}l_3^3a_2^2 + a_2l_1l_3^2 \cos^2 \varphi^b + a_2^2l_3l_2(l_2 + l_3 \cos \varphi^b) + 2a_2l_1l_2l_3 \cos \varphi^b \right], \quad (27)$$

Subsequently, the modal frequency of the main branch in branch mode is generated as

$$f_{br} = \frac{1}{2\pi} \sqrt{\frac{3EI_2}{\frac{33}{140}m_2l_2^3 + 2A_3\rho(l_2l_1^3 + \frac{1}{3}l_2^3l_1a_1^2 + a_1l_1^2l_2^2 \cos \varphi^b)}}. \quad (28)$$

where m_2 is the mass of one main branch and EI_2 is the bending stiffness of the main branch. Finally, the empirical formula of the modal frequencies for the fractal tree model with arbitrary specified orders can be derived by following the proposed derivation process.

2.4. Parameter measurement of *C. oleifera*

In the proposed fractal tree model of *C. oleifera*, any sub-branches of the tree are self-similar to the entire tree. Thus, it is possible to identify the area reduction coefficient λ and the slenderness coefficient β in Eqs. (1) and (2) by measuring a series of *C. oleifera* sub-branch specimens.

2.4.1. Location and devices

The in-situ field measurement process was implemented in Hunan Daguo Camellia oleifera research institute, which is located in Wangcheng District, Changsha City (112.8° E, 28.5° N). **10 trees of *C. oleifera* (variety: Xianglin) were randomly selected as the testing specimens.** The measurement devices and tools included a universal testing machine (model: LD23.104; maximum test force: 10 kN; manufactured by LSI SYSTEMS, Shanghai, China), a digital display vernier (resolution 0.01 mm), an angle measuring tool (resolution 0.1°), a high precision electronic balance (resolution 0.01 g; manufactured by YINGHENG, Wuxi, China), a graduated cylinder (resolution 1 mL), a tape measure and a dynamic signal analyser (model: DP906, manufactured by Data Physics, Santa Clara, USA).

2.4.2. Measurement

As shown in Fig. 9, a typical sample of the basic bifurcated unit for *C. oleifera* (variety: Xianglin) is presented. Both the diameter and the length of the trunk as well as those of two lateral branches were measured with the digital display vernier. Three reference points for measuring the branch angle are defined as the three adjacent branch points. The angle between two lateral branches was obtained using the angle measuring tool.

The density of *C. oleifera* is measured using a high-precision electronic balance and a graduated cylinder as shown in Fig. 10. The graduated cylinder is displaced on the top of the electronic balance. The Water immersion method is applied to measure the volume of branch samples by putting them into the graduated cylinder (Wang et al., 2023). As a result, the mass of each branch sample is obtained using the electronic balance. The density of each *C. oleifera* branch sample can be calculated as the ratio of the mass to the volume of each sample.

The flexural modulus of elasticity is a biomechanical property parameter of a tree, which directly contributes to the bending deformation of the branch under a certain external loading. Next, the flexural

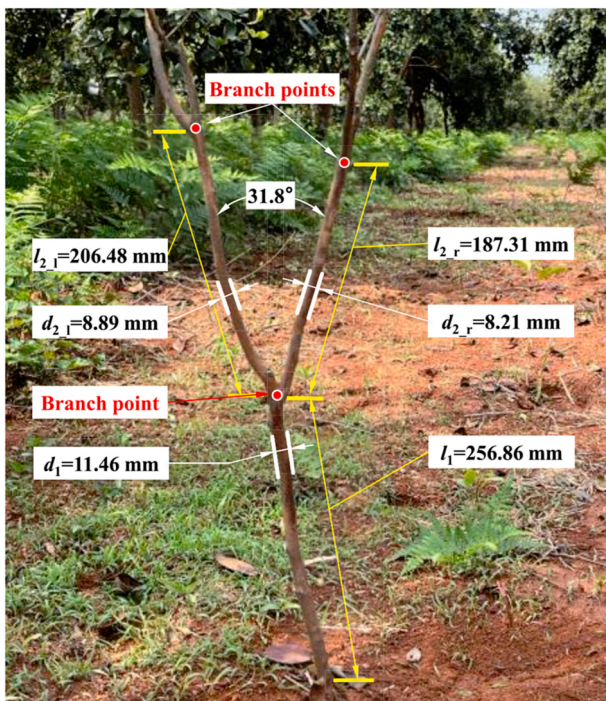


Fig. 9. Diameters and lengths of a basic bifurcated unit for *C. oleifera* (variety: Xianglin).



Fig. 10. Measurement setup for the density of Cam.

modulus of elasticity for *C. oleifera* is tested using the universal testing machine. An indenter is mounted on the moving arm of the universal testing machine. A branch of *C. oleifera* is placed on the top of the fixture. The branch bends as the indenter moves downwards along the middle of the branch. The variations of both the load and the deflection are recorded automatically. Thus, the flexural modulus of elasticity for *C. oleifera* can be calculated using the following formula.

$$E = \frac{4l^3}{3\pi d^4} \left(\frac{\Delta F}{\Delta v} \right), \quad (29)$$

where l denotes the span of the fixture, d is the branch diameter, ΔF means the variation of the external loading from the indenter and Δv

means the variation of the maximum deflection of the branch sample. Three-point bending experiments are designed for the measurement of the flexural modulus of elasticity for *C. oleifera* (Shah et al., 2017). The span of the fixture is shown in Fig. 11. The motion velocity of the indenter is set to be 10 mm/min (Wang et al., 2023).

2.5. Measurement of modal frequency for *C. oleifera*

The modal frequencies in the validation experiment and the field experiment below were measured using the dynamic signal analyser (model: DP906). The process of the measurement of the modal frequency was performed as a basic bifurcated unit in the validation experiment and a 5-year-old Y-shaped tree of *C. oleifera* oscillated in free vibration respectively.

3. Results and discussion

3.1. Diameter and length

Ten groups of measurement data involving the diameters and the lengths of the trunk and two lateral branches are included in Table 1.

3.2. Coefficients related to allometric scaling law

Using the diameters in Table 1 and then substituting into Eq. (1), the area reduction coefficient λ is calculated and listed in Table 2. By calculating the mean values, the area reduction coefficient λ of *C. oleifera* tree is finally determined to be 0.528. The logarithm of the constant e is taken as the base on both sides of Eq. (2) to calculate the slenderness coefficient β as

$$\beta = \frac{\ln \frac{d_{k+1}}{d_k}}{\ln \frac{l_{k+1}}{l_k}}. \quad (30)$$

Similarly, take the mean value of $\{\beta_1, \beta_2\}$ and the slenderness coefficient of *C. oleifera* (variety: Xianglin) is therefore identified as $\beta = 1.495$.

Since the morphological coefficients of *C. oleifera* (variety: Xianglin) are identified, the lengths and the diameters of the lateral branches can be calculated with those of the trunk by following the allometric scaling law. For example, the length and the diameter of the basic bifurcated unit in Table 1 are selected as $l_1 = 201.69$ mm and $d_1 = 15.90$ mm. Accordingly, the theoretical length and the diameter of the lateral branches are calculated as $l_{2i} = 162.89$ mm and $d_{2i} = 11.55$ mm using Eqs. (1) and (2) with the identified coefficients λ and β . The relative errors with respect to the measurement data are 3.43 % and 3.39 % for

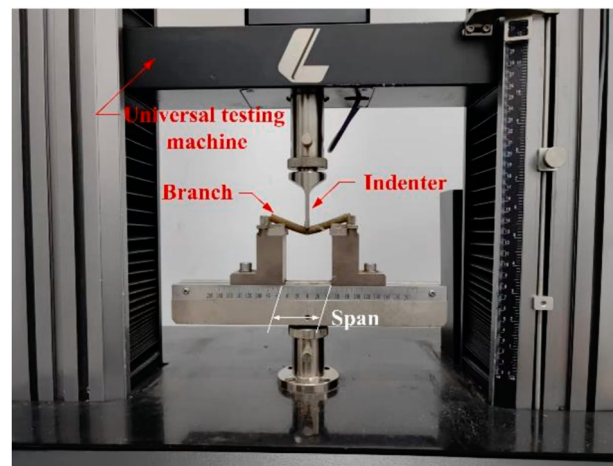


Fig. 11. Three-point bending test of a branch sample.

Table 1

Measurement data of the diameters and the lengths for the basic bifurcated unit of *C. oleifera* (variety: Xianglin).

Set	Trunk		Left branch		Right branch		Angle (°)
	Length l_1 (mm)	Diameter d_1 (mm)	Length $l_{2,1}$ (mm)	Diameter $d_{2,1}$ (mm)	Length $l_{2,r}$ (mm)	Diameter $d_{2,r}$ (mm)	
1	108.52	14.17	87.26	9.55	89.64	9.57	44.6
2	128.35	11.44	108.02	8.81	110.26	8.93	44.9
3	132.99	20.94	102.64	14.15	114.26	15.19	49.1
4	152.28	11.71	118.24	8.63	126.72	8.41	46.4
5	178.49	8.78	152.45	6.81	129.05	5.27	30.5
6	195.26	31.99	151.86	23.92	142.65	21.4	45.6
7	201.69	15.90	168.47	12.86	157.36	11.9	37.5
8	212.67	12.43	173.88	9.45	177.76	8.48	46.9
9	256.86	11.46	206.48	8.89	187.31	8.21	31.8
10	297.48	27.52	245.01	20.82	220.14	19.49	42.3

Table 2

Calculation results of area reduction coefficient λ and slenderness coefficient β .

Set	λ_1	λ_2	β_1	β_2	$\bar{\lambda}$	$\bar{\beta}$
1	0.454	0.456	1.810	2.054	0.455	1.932
2	0.593	0.609	1.515	1.630	0.601	1.573
3	0.457	0.526	1.513	2.115	0.491	1.814
4	0.543	0.516	1.206	1.802	0.529	1.504
5	0.602	0.360	1.611	1.574	0.481	1.593
6	0.559	0.448	1.156	1.281	0.503	1.219
7	0.654	0.560	1.179	1.168	0.607	1.173
8	0.578	0.465	1.361	2.133	0.522	1.747
9	0.602	0.513	1.163	1.056	0.558	1.110
10	0.572	0.502	1.438	1.146	0.537	1.292

Note: the notation $\bar{(\cdot)}$ indicates the mean value.

the lateral branch diameters d_2 , 11.3 % and 3.03 % for the lateral branch lengths. It indicates that the morphological parameters of the lateral branches generally comply with the allometric scaling law.

3.3. Density and flexural modulus of elasticity

The results of the volume and the mass of branches are recorded in Table 3. Thus, the average density of *C. oleifera* (variety: Xianglin) is obtained as $\rho = 1.033 \text{ g cm}^{-3}$, which is smaller than 1.190 g cm^{-3} mentioned in Wang (2023). The difference in the results may originate from different varieties of *C. oleifera*.

The loading and the deflection of the branches are depicted in Fig. 12. Two points in the linear variation interval of the loading curves in Fig. 12 are selected and then the ratio of ΔF to Δv is obtained. Subsequently, the flexural modulus of elasticity for *C. oleifera* is calculated using Eq. (29) and listed in Table 4. The mean value of the testing results is calculated as the flexural modulus of elasticity for *C. oleifera* (variety: Xianglin) as $E = 695 \text{ MPa}$. In comparison, the modulus of elasticity for the branch of *C. oleifera* was obtained as 630 MPa in Wang (2023), which is slightly lower than the value in the present paper.

To summarise, the morphological coefficients of *C. oleifera* (brand: Xianglin) were identified as $\lambda = 0.528, \beta = 1.495, \rho = 1.033 \text{ g/cm}^3$, the

Table 3

Calculation results of density for *C. oleifera*.

Set	Branch mass (g)	Volume (mL)	Density ($\text{g}\cdot\text{cm}^{-3}$)
1	2.42	2	1.210
2	2.82	3	0.940
3	3.16	3	1.053
4	4.08	4	1.020
5	4.70	5	0.940
6	5.21	5	1.042
7	5.97	6	0.995
8	6.51	6	1.085
9	10.12	10	1.012

angle between two lateral branches $2\varphi^b \in [30^\circ, 50^\circ]$ and $E = 695 \text{ MPa}$. These obtained parameters will be applied in the calculation of the simulation and theoretical modal frequencies.

3.4. Theoretical calculated frequency

Next, the modal frequency reflecting the trunk bending deformation in the trunk mode is calculated using the proposed method and compared with the method mentioned in Oguamanam (2003). Substitute the morphological coefficients of the basic bifurcated unit into Eq. (16) and the resultant modal frequencies are obtained with the variance of the angle φ^b . The modal frequencies and the corresponding relative errors are listed in Table 5. It shows that the modal frequencies are highly related to the angle φ^b . In addition, the relative errors of the modal frequency calculated from the proposed method and the method (Oguamanam, 2003) are less than 3 %.

3.5. Finite element simulation

A finite element model in ANSYS Mechanical ADPL 2020 software is created with the angle $\varphi^b = 20^\circ$ shown in Fig. 13. The morphological coefficients of the finite element model are selected as the same as those in the previous theoretical calculation. The modal frequency in the trunk mode with ANSYS is obtained as 13.373 Hz with the angle $\varphi^b = 20^\circ$, which is very close to that calculated by the proposed theoretical method. The modal shape associated with the modal frequency in the trunk mode is represented as the bending deformation of the trunk with two lateral branches as rigid bodies as depicted in Fig. 13b.

Subsequently, the modal frequencies of the basic bifurcated unit of *C. oleifera* with different branch angles are obtained and compared with the theoretical results in Fig. 14. The results reveal that the angle φ_b contributes to the calculation of the modal frequency in the trunk mode. The modal frequency increases gradually as the branch angle becomes larger. More importantly, the value from the proposed theoretical method matches the value from ANSYS software very well with the maximum relative errors less than 0.2 %.

Furthermore, another finite element model is created for three basic bifurcated units with the same branching structure in Malhi et al. (2018). The modal shapes of the corresponding modal frequencies based on ANSYS software are shown in Fig. 15. It demonstrates that in trunk mode only the trunk bends and all the branches move as a rigid body, while the trunk remains still and only the secondary branches bend in branch mode.

3.6. Empirical frequency

Based on the results from the finite element analysis, two coefficients in Eq. (22) and Eq. (26) are determined to be $a_1 = 1.633 + 0.0426 \frac{l_1 \cos \varphi^b}{l_2}$ and $a_2 = 1.633 + 0.0426 \frac{l_1 \cos \varphi^b}{l_3} + 0.1704 \frac{l_2}{l_3}$. The modal frequencies of the basic bifurcated unit in trunk mode with different

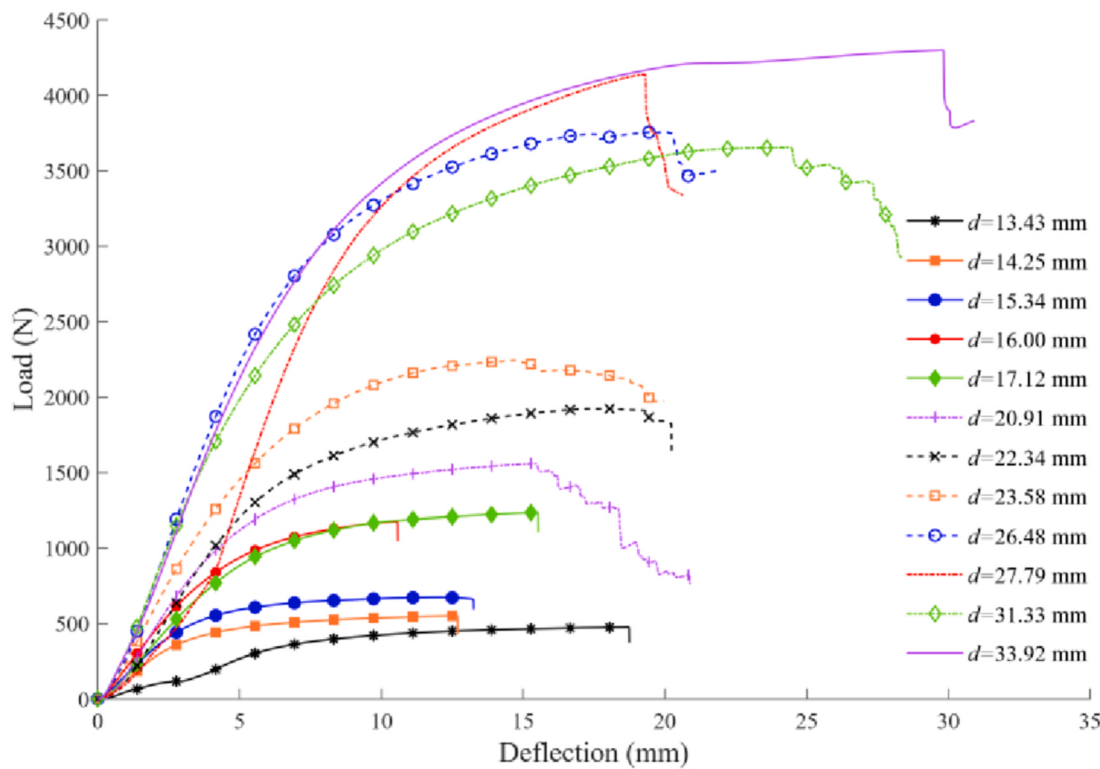


Fig. 12. Deflection-load results of branch bending test.

Table 4
Calculation results of the flexural modulus of elasticity for *C. oleifera*.

Set	Branch diameter (mm)	Flexural modulus of elasticity (MPa)
1	13.43	543.27
2	14.25	873.3
3	15.34	738.45
4	16.00	796.76
5	17.12	537.58
6	20.91	850.74
7	22.34	696.87
8	23.58	657.54
9	26.48	617.6
10	27.79	556.63
11	31.33	697.31
12	33.92	777.56

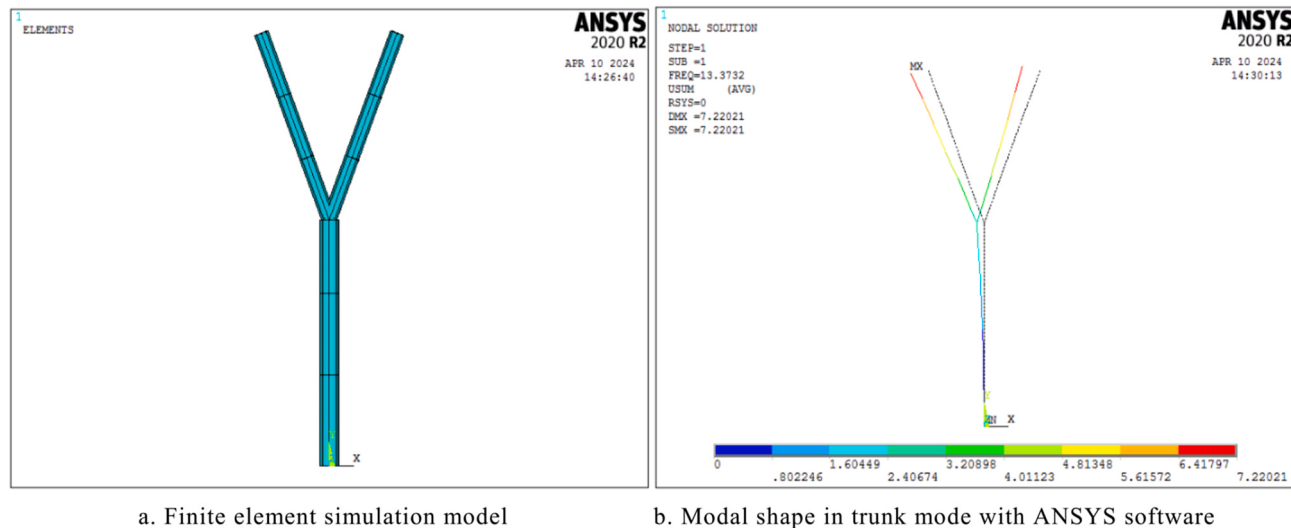
Table 5
Modal frequencies of the basic bifurcated unit in the trunk mode by theoretical methods.

φ^b (°)	Modal frequency in the trunk mode (Hz)		
	The proposed method	The method (Oguamanam, 2003)	Relative error (%)
10	13.24	13.64	2.93
15	13.29	13.69	2.92
20	13.37	13.77	2.91
25	13.47	13.87	2.91
30	13.59	13.99	2.90
35	13.73	14.14	2.88
40	13.90	14.31	2.87
45	14.10	14.51	2.85
50	14.32	14.74	2.83
55	14.58	15.00	2.81
60	14.86	15.29	2.79
65	15.18	15.61	2.76

branch angles φ^b are calculated from the derived empirical formula. Subsequently, they are used to compare with the results from both the simulation results using ANSYS software and the proposed theoretical method in Table 6. It is observed that the relative error of the modal frequency from the empirical formula is higher than that from the proposed theoretical method. However, the obtained modal frequency by the empirical formula is also very close to the simulation results with the maximum relative error less than 0.8 %. Thus, the empirical formula is a feasible alternative to the proposed theoretical method to obtain modal frequencies with high computational accuracy and easy-to-use mathematical operations.

As aforementioned in Sect. 3, the motion of two lateral branches for a basic bifurcated unit in trunk mode is regarded as a rigid body motion of two lateral branches. Similarly, all branches except for the trunk of the fractal tree in trunk mode vibrate as a single rigid body motion. Furthermore, the modal frequencies both in the trunk mode and in the branch mode for the three basic bifurcated units are obtained from the proposed empirical formulas. The detailed comparison between the empirical frequencies and the simulation frequencies from ANSYS software is included in Table 7. The maximum relative error for the modal frequencies in the trunk mode is less than 1.7 % among the branch angle range from 10 ° to 65 °. Moreover, the maximum relative error in the branch mode is much less than that in the trunk mode, which is less than 0.61 %. The relative error for the modal frequency in the branch mode is always less than that in the trunk mode with the same dimension and the branch angle. Nevertheless, these two empirical formulas are verified well for the determination of the modal frequencies in trunk mode and branch mode with high accuracy. More importantly, it shows that the modal frequency in branch mode is around two times higher than that in trunk mode, which means that the harvesting frequency should be two times higher as the trunk vibrates than as the branches merely vibrate.

It is worth noting that the resultant modal frequency for the three basic bifurcated unit in trunk mode is in the range of 6.8–8.4 Hz, which varies due to the angle φ^b . This range of modal frequency is close to the existing experimental results of 6–7 Hz with those presented in the articles (Du, Chen, et al., 2022; Du, Shen, et al., 2022; Wu et al., 2022; Yan



a. Finite element simulation model

b. Modal shape in trunk mode with ANSYS software

Fig. 13. Finite element model and the simulation modal shape in the trunk mode of the bifurcated basic unit.

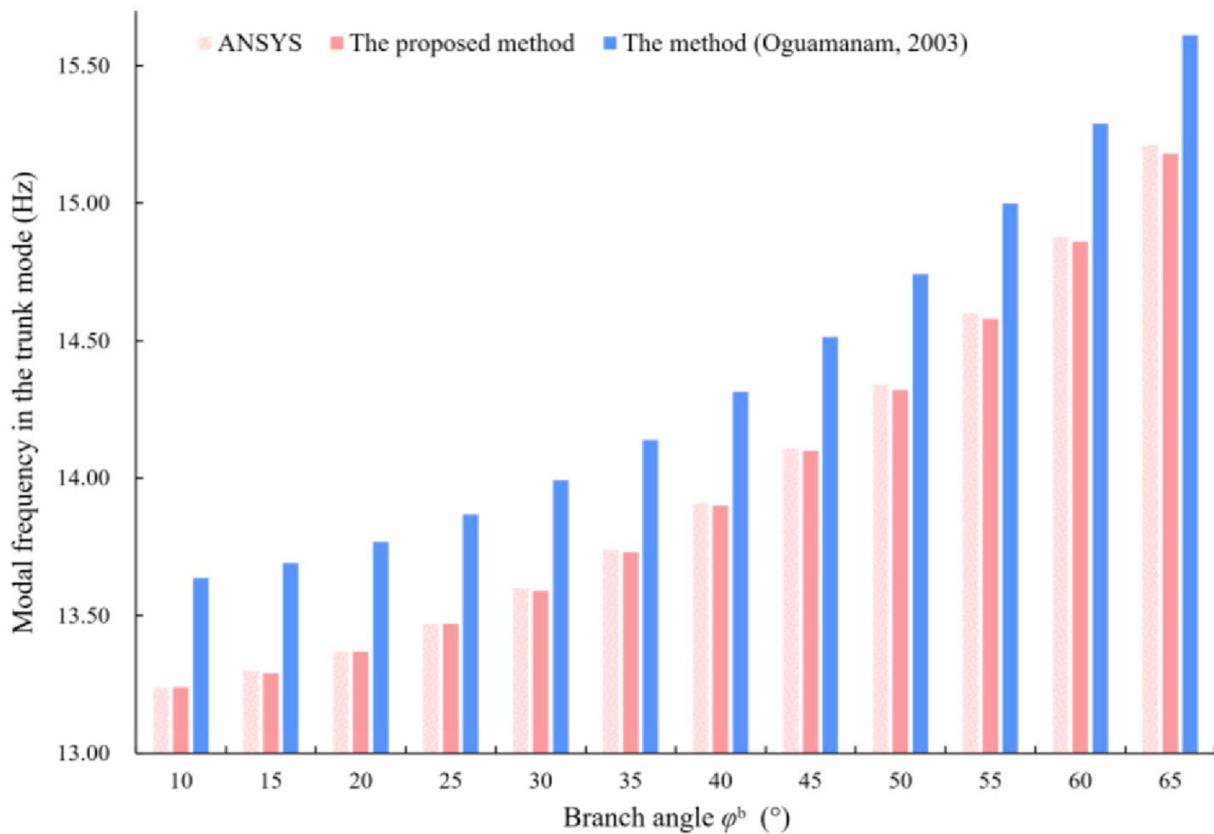
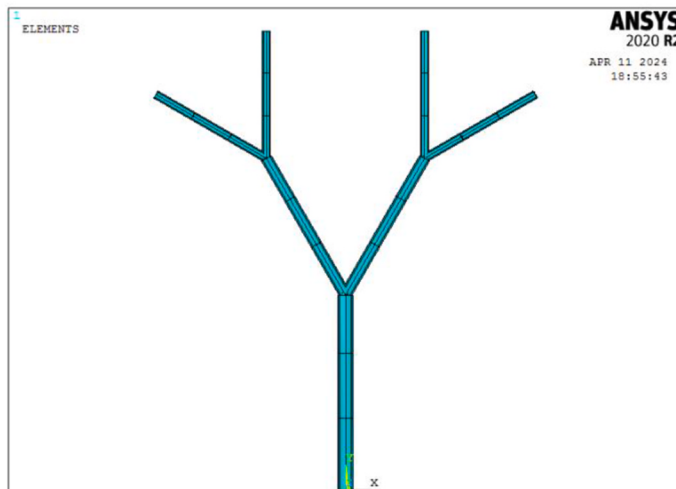
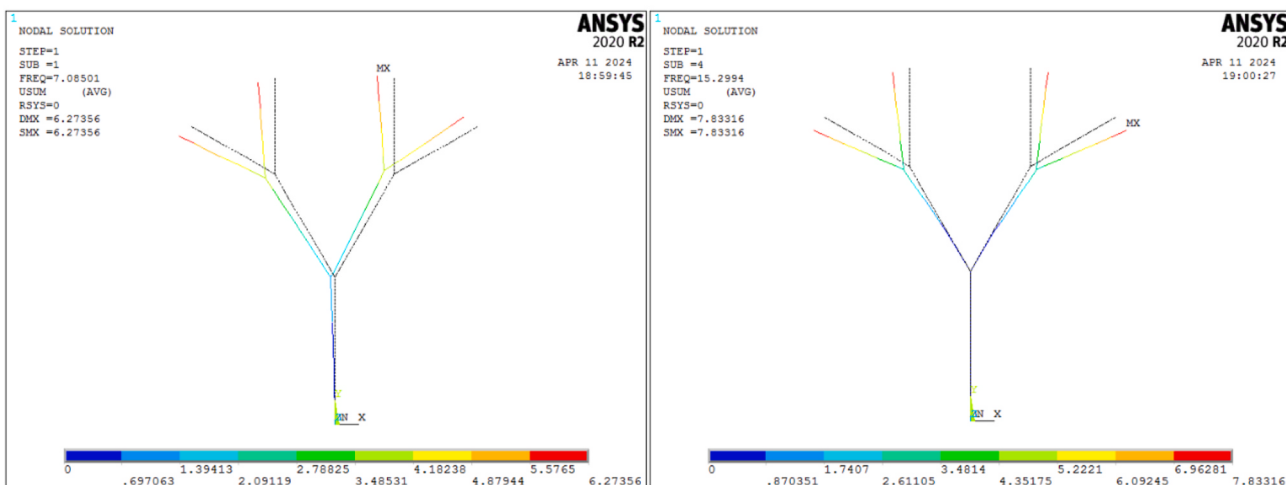


Fig. 14. Comparison of modal frequencies in the trunk mode from both ANSYS and theoretical calculation methods.



a. Finite element simulation model



b. Modal shape in trunk mode

c. Modal shape in branch mode

Fig. 15. Finite element model and the simulation modal shapes of the three bifurcated basic units.

Table 6

Modal frequencies of the basic bifurcated unit in trunk mode by ANSYS software and the proposed empirical formula.

ϕ^b (°)	Modal frequency in trunk mode (Hz)		Relative error (%)		
	ANSYS software	Empirical formula	Proposed theoretical method	Empirical	Theoretical
10	13.24	13.30	13.24	0.53	0
15	13.30	13.36	13.29	0.45	0.08
20	13.37	13.44	13.37	0.52	0
25	13.47	13.54	13.47	0.52	0
30	13.60	13.67	13.59	0.51	0.07
35	13.74	13.82	13.73	0.58	0.07
40	13.91	14.00	13.90	0.65	0.07
45	14.11	14.20	14.10	0.64	0.07
50	14.34	14.44	14.32	0.70	0.14
55	14.60	14.70	14.58	0.68	0.14
60	14.88	15.00	14.86	0.81	0.13
65	15.21	15.32	15.18	0.72	0.20

Table 7

Comparison of modal frequencies of the three basic bifurcated units in the trunk mode and the branch mode.

ϕ^b (°)	Modal frequency (Hz)					
	Trunk mode			Branch mode		
	ANSYS	Empirical formula Eq. (26)	Relative error (%)	ANSYS	Empirical formula Eq. (28)	Relative error (%)
10	6.80	6.87	0.99	14.91	14.82	0.61
15	6.85	6.91	0.92	14.97	14.88	0.59
20	6.91	6.98	0.96	15.05	14.97	0.53
25	6.99	7.06	1.00	15.16	15.08	0.50
30	7.09	7.16	1.02	15.30	15.23	0.48
35	7.20	7.29	1.20	15.46	15.40	0.42
40	7.34	7.43	1.25	15.66	15.59	0.42
45	7.50	7.60	1.34	15.88	15.82	0.36
50	7.69	7.79	1.35	16.13	16.08	0.30
55	7.90	8.01	1.45	16.42	16.38	0.27
60	8.13	8.26	1.63	16.75	16.70	0.27
65	8.40	8.54	1.70	17.11	17.07	0.23

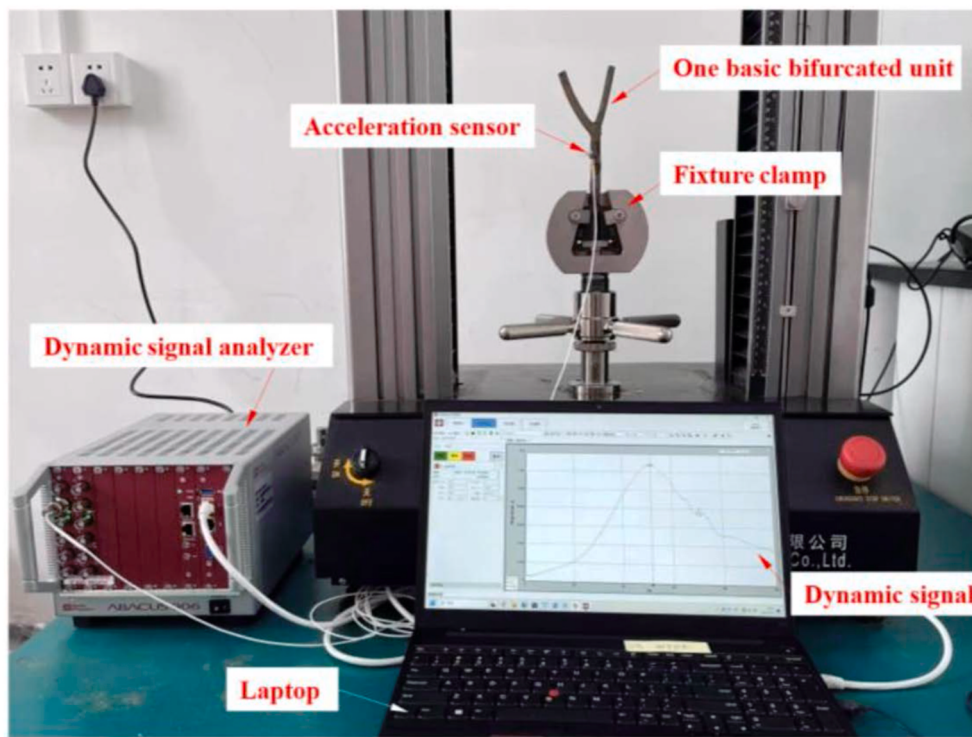


Fig. 16. Experiment layout with one basic bifurcated unit.

Table 8

Dimensions of the diameters and the lengths for the basic bifurcated unit in test (variety: Xianglin).

Trunk	Left branch			Right branch		Angle (°)
	Length l_1 (m)	Diameter d_1 (m)	Length $l_{2,1}$ (m)	Diameter $d_{2,1}$ (m)	Length $l_{3,r}$ (m)	Diameter $d_{3,r}$ (m)
0.08423	0.01120	0.06876	0.00945	0.06892	0.00794	40.7

et al., 2023). The discrepancy between the obtained modal frequencies and the existing results is caused by the simplification of our proposed fractal tree model from a 3-dimensional complex tree to a 2-dimensional structured tree model.

In addition, the empirical formula for the modal frequency is merely applied to the fractal tree model with three basic bifurcated units. If more sub-branches are considered, the modal frequency in both trunk mode and branch modes will decrease due to the increase of the moment of inertia for additional branches.

3.7. Validation experiment

As shown in Fig. 16, the validation experiment layout for a basic bifurcated unit includes a fixture clamp, an acceleration sensor, a dynamic signal analyser and a laptop. The fixture clamp is applied to grip the bottom of the trunk. The acceleration sensor is attached to the top of the trunk and connected to the dynamic signal analyser. The laptop is used to record and show dynamic acceleration signals through an Ethernet cable.

The validation experiment process is implemented as recording the acceleration signal at the attachment point on the trunk after a sudden release of the lateral branch away from its static equilibrium position. The dimensions of the experimental sample for *C. oleifera* (variety: Xianglin) are measured in Table 8.

The testing results between the frequency and the acceleration were obtained in Fig. 17, where the modal frequency in the trunk mode was identified as 51.50 Hz. Based on Table 8, the empirical modal frequency in the trunk mode for the basic bifurcated unit is calculated as 54.28 Hz and the modal frequency with the proposed theoretical method is obtained as 54.01 Hz. The relative error between the experimental frequency and the empirical frequency is 5.4 %. It is clearly noted that the experimental modal frequency was in good agreement with that from the empirical formula and the proposed theoretical method. The main reason for the discrepancy in the modal frequency is that the left branch diameter of the experimental sample was larger than the theoretical diameter following the allometric scaling law.

3.8. Field experiment

To validate the efficiency of the obtained modal frequency, a 5-year-old Y-shaped tree of *C. oleifera* in Fig. 18 was selected from the Specialty Oil Crop (*C. oleifera*) Full Mechanization Research Centre in Hunan, China. In the field experiment setting, the designated tree was cut from the roots and fixed with a three-jaw chuck in the lab to eliminate the effect of soil movement. The length and the diameter of the trunk were measured as $l_1 = 0.427$ m and $d_1 = 0.035$ m. Following the allometric scaling law, the diameter of the main branch is calculated as $l_2 = 0.345$ m and $d_2 = 0.0254$ m.

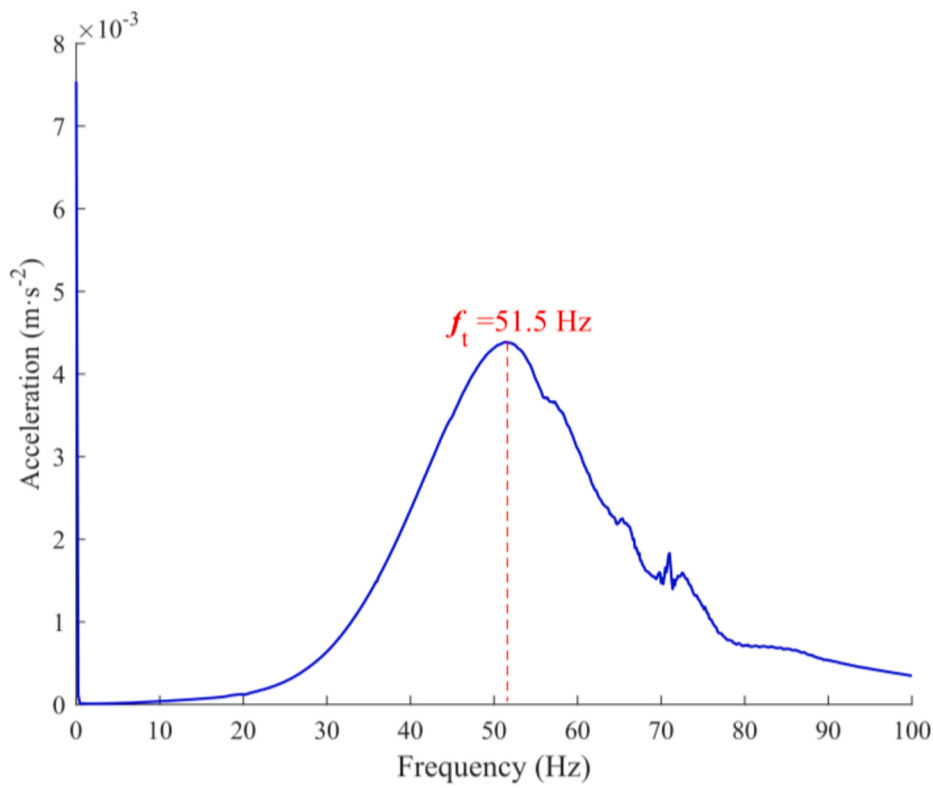


Fig. 17. Frequency-acceleration testing results.



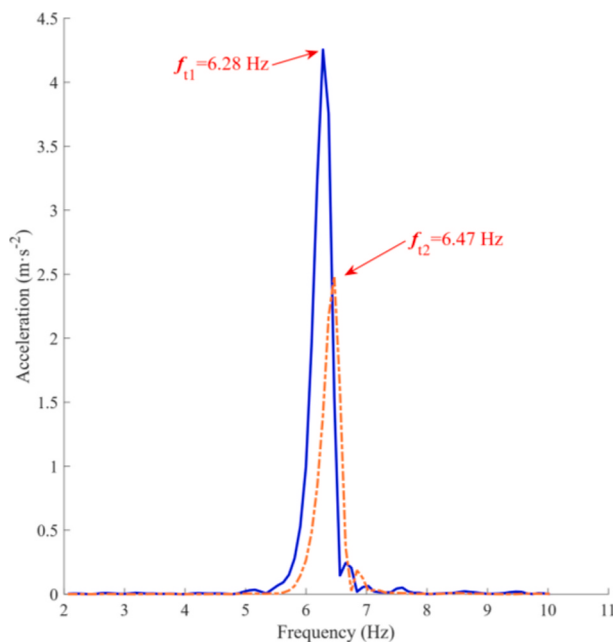
Fig. 18. Field experiment setting.

Table 9

Modal frequencies of the Y-shaped tree in trunk mode identified by experiments and from the proposed empirical formula.

φ^b (°)	Modal frequency in trunk mode (Hz)		Relative error (%)			
	Empirical formula	Experiments				
		1st test	2nd test			
21.2	6.61	6.28	6.47	5.25	2.16	Relative error (%)

The empirical modal frequency in trunk mode for the tree is calculated as $f_t = 6.61 \text{ Hz}$ using Eq. (23). The experimental modal frequency was measured using the dynamic signal analyser during the same testing process as Subsect. 3.7. The experimental frequencies identified in two tests and the empirical modal frequency are listed in Table 9 with relative errors of less than 6 %. It can be explained that the architecture of the specified tree was more complex than the proposed Y-shaped simplified tree model. The dynamic response of the test tree was recorded at the actuation frequency of 6.6 Hz, and a large amplitude of vibration was observed in the uploaded video.



3.9. Limitations of the proposed model

Although the proposed formulas have been well verified by the experiments, it is worth noting that there are some limitations in the proposed model. Firstly, the simplified fractal tree model of *C. oleifera* is established in a 2-dimensional plane rather than a 3-dimensional space. Secondly, the fractal tree model only exists in mathematics in comparison to more complex tree architectures in real conditions. Thirdly, the soil movement beneath the trunk during free vibration is ignored in the present model, which can be regarded as a considerable passive mass damper for the tree model. These limitations may be solved by incorporating the finite element method in the present theoretical framework.

4. Conclusions

This paper presents a simplified fractal tree model of *C. oleifera* based on its sympodial branching mode, where the general allometric scaling

Appendix

The extended Hamilton's principle is applied to the basic bifurcated unit of *C. oleifera* as

$$\int_{t_1}^{t_2} (\delta T - \delta V + \delta W) dt = 0, \quad (\text{A-1})$$

where the variation of the kinetic energy $\delta T = \delta T_{\text{trunk}} + \delta T_{l_2}$. In addition, the variation of the virtual work is assumed to be zero in free vibration.

Using Eq. (18), the variation of the elastic potential energy is yielded as

$$\delta V = \frac{3EI}{l_1} \theta_o \delta \theta_o. \quad (\text{A-2})$$

Based on Eqs. (19)–(22), the variation of the kinetic energy is expressed as

$$\delta T = \frac{33}{140} ml_1^2 \dot{\theta}_o \delta \dot{\theta}_o + 2A_2 \rho \left(l_2 l_1^2 + \frac{1}{3} l_2^3 a_1^2 + a_1 l_1 l_2^2 \cos \varphi^b \right) \dot{\theta}_o \delta \dot{\theta}_o. \quad (\text{A-3})$$

By substituting Eqs. (A-2) and (A-3) into Eq. (A-1), the following equation is obtained

$$\int_{t_1}^{t_2} \left[\frac{33}{140} ml_1^2 \dot{\theta}_o \delta \dot{\theta}_o + 2A_2 \rho \left(l_2 l_1^2 + \frac{1}{3} l_2^3 a_1^2 + a_1 l_1 l_2^2 \cos \varphi^b \right) \dot{\theta}_o \delta \dot{\theta}_o - \frac{3EI}{l_1} \theta_o \delta \theta_o \right] dt = 0. \quad (\text{A-4})$$

law for biological architecture is adopted to establish the relationship among branch dimensions in hierarchical order. It concludes that the area reduction coefficient and the slenderness coefficient of *C. oleifera* (variety: Xianglin) are identified as 0.528 and 1.495 respectively. Two empirical formulas are derived for the simplified fractal tree model to calculate the modal frequencies. Comparison between the empirical frequencies and the simulation frequencies from ANSYS software shows that the relative errors are less than 2 %. Furthermore, the relative errors between the empirical frequencies and the experimentally identified frequencies are less than 6 %, which demonstrates the feasibility of the proposed empirical formulas. In addition, the results show that the modal frequency in branch mode is generally around two times higher than that in trunk mode, which leads to the guidance for the selection of suitable vibrational frequencies in forestry fruit harvesting. Our next research direction will investigate more accurate frequencies using the finite element method for different complex tree architectures and simplify the results into an empirical model in the theoretical framework.

CRediT authorship contribution statement

Lewei Tang: Writing – original draft, Visualization, Validation, Project administration, Methodology, Investigation, Funding acquisition, Conceptualization. **Huiyu Zhang:** Visualization, Validation, Data curation. **Shiyi Zhang:** Validation, Software, Formal analysis, Data curation. **Rui Pan:** Resources, Investigation, Data curation. **Mingliang Wu:** Writing – review & editing, Supervision, Resources, Project administration, Funding acquisition.

Declaration of competing interest

The authors declare that they have no known competing financial interests or personal relationships that could have appeared to influence the work reported in this paper.

Acknowledgments

This work in this paper was supported by the National Natural Science Foundation of China (Grant No. 52305020), the Provincial Natural Science Foundation of Hunan (Grant No. 2025JJ50176), the China Postdoctoral Science Foundation (Grant No. 2023M741142) and National Funded Postdoctoral Researcher Program (Grant No. GZC20230776).

Considering that $\dot{\theta}_0 \delta \dot{\theta}_0 = \ddot{\theta}_0 \delta \theta_0$, Eq. (23) is finally yielded.

Appendix B. Supplementary data

Supplementary data related to this article can be found at <https://doi.org/10.1016/j.biosystemseng.2025.104296>.

References

- Bejan, A., Lorente, S., & Lee, J. (2008). Unifying constructal theory of tree roots, canopies and forests. *Journal of Theoretical Biology*, 254(3), 529–540. <https://doi.org/10.1016/j.jtbi.2008.06.026>
- Camposeo, S., Vicino, F., Vivaldi, G., & Pascuzzi, S. (2023). Re-shaping pruning improves the dynamic response of centuries-old olive trees to branch-shaker vibrations application. *Frontiers in Plant Science*, 14. <https://doi.org/10.3389/fpls.2023.1155120>
- Castro-Garcia, S., Blanco-Roldan, G. L., & Gil-Ribes, J. A. (2012). Vibrational and operational parameters in mechanical cone harvesting of stone pine (*Pinus pinea* L.). *Biosystems Engineering*, 112(4), 352–358. <https://doi.org/10.1016/j.biosystemseng.2012.05.007>
- Chen, S., Zou, X., Zhou, X., Xiang, Y., & Wu, M. (2023). Study on fusion clustering and improved YOLOv5 algorithm based on multiple occlusion of *C. oleifera* fruit. *Computers and Electronics in Agriculture*, 206, Article 107706. <https://doi.org/10.1016/j.compag.2023.107706>
- Droukas, L., Doulgeri, Z., Tsakiridis, N. L., et al. (2023). A survey of robotic harvesting systems and enabling technologies. *Journal of Intelligent and Robotic Systems*, 107(2), 21. <https://doi.org/10.1007/s10846-022-01793-z>
- Du, X., Han, X., Shen, T., et al. (2024). Natural frequency identification model based on BP neural network for *C. oleifera* fruit harvesting. *Biosystems Engineering*, 237, 38–49. <https://doi.org/10.1016/j.biosystemseng.2023.11.012>
- Du, X., Ning, C., He, L., Qian, Y., Zhang, G., & Yao, X. (2022). Design and test of crawler-type high clearance *C. oleifera* fruit vibratory harvester. *Transactions of the Chinese Society for Agricultural Machinery*, 53(7), 113–121. <https://doi.org/10.6041/j.issn.1000-1298.2022.07.011> (in Chinese).
- Du, X., Shen, T., Chen, K., Zhang, G., Yao, X., Chen, J., & Cao, Y. (2022). Simulation study and field experiments on the optimal canopy shaking action for harvesting *C. oleifera* fruits. *Journal of Agricultural Engineering*, 53(3), 1245. <https://doi.org/10.4081/jae.2022.1245>
- Du, X., Shen, T., Zhao, L., Zhang, G., Hu, A., Fang, S., Cao, Y., & Yao, X. (2021). Design and experiment of the comb-brush harvesting machine with variable spacing for oil-tea camellia fruit. *International Journal of Agricultural and Biological Engineering*, 14 (1), 172–177. <https://doi.org/10.25165/j.ijabe.20211401.5703>
- Eloy, C. (2011). Leonardo's rule, self-similarity, and wind-induced stresses in trees. *Physical Review Letters*, 107, Article 258101. <https://doi.org/10.1103/PhysRevLett.107.258101>
- Gao, L., Jin, L., Liu, Q., Zhao, K., Lin, L., Zheng, J., Li, C., Chen, B., & Shen, Y. (2024). Recent advances in the extraction, composition analysis and bioactivity of Camellia (*C. oleifera* Abel.) oil. *Trends in Food Science & Technology*, 143, Article 104211. <https://doi.org/10.1016/j.tifs.2023.104211>
- Gao, C., Yuan, D., Wang, B., Yang, Y., Liu, D., & Han, Z. (2015). A cytological study of anther and pollen development in *C. oleifera*. *Genetics and Molecular Research*, 14(3), 8755–8765. <https://doi.org/10.4238/2015.July.31.24>
- Hoshyarmanesh, H., Dastgerdi, H. R., Ghodsi, M., Khandan, R., & Zareinia, K. (2017). Numerical and experimental vibration analysis of olive tree for optimal mechanized harvesting efficiency and productivity. *Computers and Electronics in Agriculture*, 132, 34–48. <https://doi.org/10.1016/j.compag.2016.11.014>
- James, K. R., Haritos, N., & Ades, P. K. (2006). Mechanical stability of trees under dynamic loads. *American Journal of Botany*, 93(10), 1522–1530. <https://doi.org/10.3732/ajb.93.10.1522>
- Jiao, H., Tang, A., Ma, C., Li, Y., Wang, L., & Li, C. (2024). Modelling and numerical simulation of a concentrated mass-based branch vibration. *Scientia Horticulturae*, 330, Article 113028. <https://doi.org/10.1016/j.scienta.2024.113028>
- Lang, Z. (2008). A one degree of freedom damped fruit tree model. *Transactions of the ASABE*, 51(3), 823–829. <https://doi.org/10.13031/2013.24520>
- Lang, Z., & Csorba, L. (2015). A two degree of freedom damped fruit tree model. *International Agricultural Engineering Journal: CIGR Journal*, 17(3), 335–341. <https://cigrjournal.org/index.php/Ejournal/article/view/3298>
- Li, B., Lu, H., Lü, E., Li, J., Qiu, G., Yin, H., & Ma, Y. (2018). Characterizing energy transfer of litchi branches and working parameters of destemmed vibrational picking. *Transactions of the Chinese Society of Agricultural Engineering*, 34(8), 18–25. <https://doi.org/10.11975/j.issn.1002-6819.2018.08.003> (in Chinese).
- Loong, C. N., & Dimitrakopoulos, E. G. (2023). Modal properties of fractal sypodial trees: Insights and analytical solutions using a group tree modeling approach. *Applied Mathematical Modelling*, 115, 127–147. <https://doi.org/10.1016/j.apm.2022.10.048>
- Loong, C. N., Siu, H. M., & Dimitrakopoulos, E. G. (2024). Modal properties of fractal trees as recursive analytical solutions. *Journal of Sound and Vibration*, 572, Article 118164. <https://doi.org/10.1016/j.jsv.2023.118164>
- Lopez, D., Michelin, S., & Langre, E. D. (2011). Flow-induced pruning of branched systems and brittle reconfiguration. *Journal of Theoretical Biology*, 284, 117–124. <https://doi.org/10.1016/j.jtbi.2011.06.027>
- Luan, F., Zeng, J., Yang, Y., He, X., Wang, B., Gao, Y., & Zeng, N. (2020). Recent advances in *C. oleifera* Abel: A review of nutritional constituents, biofunctional properties, and potential industrial applications. *Journal of Functional Foods*, 75, Article 104242. <https://doi.org/10.1016/j.jff.2020.104242>
- Ma, R., Homayouni, T., Toudeshki, A., Ehsani, R., & Zhang, X. (2022). An experimental study and mathematical modeling of vibration transfer in pistachio trees using an inertia-type trunk shaker and field-adapted wireless sensors. *Shock and Vibration*, 2022(1), Article 9966848. <https://doi.org/10.1155/2022/9966848>
- Malhi, Y., Tobias, J., Lisa, P., Alvaro, L., Alexander, S., Martin, H., Kim, C., Harm, B., & Mathias I, D. (2018). New perspectives on the ecology of tree structure and tree communities through terrestrial laser scanning. *Interface Focus*, 8(2), Article 20170052. <https://doi.org/10.1098/rsfs.2017.0052>
- Murphy, K. D., & Rudnicki, M. (2012). A physics-based link model for tree vibrations. *American Journal of Botany*, 99(12), 1918–1929. <https://doi.org/10.3732/ajb.1200141>
- Niu, Z., Xu, Z., Deng, J., Zhang, J., Pan, S., & Mu, H. (2022). Optimal vibration parameters for olive harvesting from finite element analysis and vibration tests. *Biosystems Engineering*, 215, 228–238. <https://doi.org/10.1016/j.biosystemseng.2022.01.002>
- Oguamanam, D. C. D. (2003). Free vibration of beams with finite mass rigid tip load and flexural-torsional coupling. *International Journal of Mechanical Sciences*, 45(6–7), 963–979. <https://doi.org/10.1016/j.ijmecsci.2003.09.014>
- Quan, W., Wang, A., Gao, C., & Li, C. (2022). Applications of Chinese *C. oleifera* and its by-products: A review. *Frontiers in Chemistry*, 10, Article 921246. <https://doi.org/10.3389/fchem.2022.921246>
- Rodriguez, M., Langre, E. D., & Moulia, B. (2008). A scaling law for the effects of architecture and allometry on tree vibration modes suggests a biological tuning to modal compartmentalization. *American Journal of Botany*, 95(12), 1523–1537. <https://doi.org/10.3732/ajb.0800161>
- Shah, D., Reynolds, T., & Ramage, M. (2017). The strength of plants: Theory and experimental methods to measure the mechanical properties of stems. *Journal of Experimental Botany*, 68(16), 4497–4516. <https://doi.org/10.1093/jxb/erx245>
- Sola-Guirado, R., Luque-Mohedano, R., Tombesi, S., & Blanco-Roldan, G. (2022). Effect of leaves in the dynamic response of olive tree branches and their computational model. *Computers and Electronics in Agriculture*, 203, Article 107490. <https://doi.org/10.1016/j.compag.2022.107490>
- Spatz, H. C., Bruchert, F., & Pfisterer, J. (2007). Multiple resonance damping or how do trees escape dangerous large oscillations? *American Journal of Botany*, 94(10), 1603–1611. <https://doi.org/10.3732/ajb.94.10.1603>
- Tang, L., Gouttefarde, M., Doria, A., Sun, H., Wang, H., & Zhou, C. (2022). Analysis and verification of cable pretension effect on the buckling load of a single-link flexible mechanism. *Applied Mathematical Modelling*, 104, 499–516. <https://doi.org/10.1016/j.apm.2021.11.034>
- Tang, L., Gouttefarde, M., Sun, H., Yin, L., & Zhou, C. (2021). Dynamic modelling and vibration suppression of a single-link flexible manipulator with two cables. *Mechanism and Machine Theory*, 162, Article 104347. <https://doi.org/10.1016/j.mechmachtheory.2021.104347>
- Theckes, B., Langre, E. D., & Boutilhon, X. (2011). Damping by branching: A bioinspiration from trees. *Bioinspiration & Biomimetics*, 6(4), Article 046010. <https://doi.org/10.1088/1748-3182/6/4/046010>
- Wang, J. (1965). Mechanical coffee harvesting (Part A). *Transactions of the ASAE*, 8(3), 400–402. <https://doi.org/10.13031/2013.40529>
- Wang, R., Fang, D., Wu, C., et al. (2024). Dynamic response of *C. oleifera* fruit-branch based on mathematical model and high-speed photography. *Biosystems Engineering*, 237, 232–241. <https://doi.org/10.1016/j.biosystemseng.2023.12.010>
- Wang, F., Zhou, J., Miao, Z., Liu, Y., Feng, H., Lei, Y., Wang, T., & Xiong, C. (2023). Simulation and experimental analysis of *C. oleifera* fruit shedding based on finite element explicit dynamics. *Bioresources*, 18(4), 8394–8408. <https://doi.org/10.15376/biores.18.4.8394-8408>
- Weng, L., & Xu, L. (2013). Analysis on mechanical model assumption of Y-trellis trees. *Journal of Agricultural Mechanization Research*, 4, 19–24. <https://doi.org/10.13427/j.cnki.jnjyj.2013.04.057>
- West, G. B., Brown, J. H., & Enquist, B. J. (1997). A general model for the origin of allometric scaling laws in biology. *Science*, 276, 122–126. <https://doi.org/10.1126/science.276.5309.122>
- West, G. B., Brown, J. H., & Enquist, B. J. (1999). The fourth dimension of life: Fractal geometry and allometric scaling of organisms. *Science*, 284, 677–1679. <https://doi.org/10.1126/science.284.5420.1677>
- Wu, D., Zhao, E., Jiang, S., Wang, W., Yuan, J., & Wang, K. (2022). Optimization and experiment of canopy vibration parameters of *C. oleifera* based on energy transfer characteristics. *Transactions of the Chinese Society for Agricultural Machinery*, 53(8), 23–33. <https://doi.org/10.6041/j.issn.1000-1298.2022.08.003> (in Chinese).
- Yan, F., Li, X., Yang, Y., Huang, G., Zhang, Y., & Yang, F. (2023). Design and experiment of hand-held impacting comb-type *C. oleifera* fruit harvester. *Transactions of the Chinese Society for Agricultural Machinery*, 54(12), 129–140 (in Chinese). <https://doi.org/10.6041/j.issn.1000-1298.2023.12.012>
- Zhang, J., Ying, Y., & Yao, X. (2019). Effects of turning frequency on the nutrients of *C. oleifera* shell co-compost with goat dung and evaluation of co-compost maturity. *PLoS One*, 14(9), Article e0222841. <https://doi.org/10.1371/journal.pone.0222841>
- Zhang, F., Zhu, F., Chen, B., Su, E., Chen, Y., & Cao, F. (2022). Composition, bioactive substances, extraction technologies and the influences on characteristics of *C. oleifera*

- oil: A review. *Food Research International*, 156, Article 111159. <https://doi.org/10.1016/j.foodres.2022.111159>
- Zheng, Z., Hu, Y., Guo, T., Qiao, Y., He, Y., Zhang, Y., & Huang, Y. (2023). AGHRNet: An attention ghost-HRNet for confirmation of catch-and-shake locations in jujube fruits vibration harvesting. *Computers and Electronics in Agriculture*, 210, Article 107921. <https://doi.org/10.1016/j.compag.2023.107921>
- Zheng, Y., Jiang, S., Chen, B., Lü, H., Wan, C., & Kang, F. (2020). Review on technology and equipment of mechanization in hilly orchard. *Transactions of the Chinese Society for Agricultural Machinery*, 51(11), 1–20. <https://doi.org/10.6041/j.issn.1000-1298.2020.11.001> (in Chinese).
- Zhou, J., Xu, L., Zhao, J., Hang, X., & Zhou, H. (2022). Effective excitation conditions for the intense motion of the ginkgo seed-stem system during mechanical vibration harvesting. *Biosystems Engineering*, 239–248. <https://doi.org/10.1016/j.biosystemseng.2022.01.014>, 2022.